THE POLAR REGIONS OF CASSIOPEIA A: THE AFTERMATH OF A GAMMA-RAY BURST?

J. Martin Laming,[1] Una Hwang,[2] Balint Radics,[3] Gergely Lekli,[3] and Endre Takács[3]

ABSTRACT

Are the polar regions of Cas A the aftermath of a gamma-ray burst? Probably not, but it is interesting nevertheless to investigate just how close Cas A might have come to generating such an event. Focusing on the northeast jet filaments, we analyze the polar regions of the recently acquired very deep 1 Ms *Chandra* X-ray observation. We infer that the so-called "jet" regions are indeed due to jets emanating from the explosion center and not due to polar cavities in the circumstellar medium at the time of explosion. We place limits on the equivalent isotropic explosion energy in the polar regions (around 2.3×10^{52} ergs) and the opening angle of the X-ray–emitting ejecta (around $7°$), which give a total energy in the northeast jet of the order of 10^{50} ergs, an order of magnitude or more lower than inferred for "typical" GRBs. While the Cas A progenitor and explosion exhibit many of the features associated with GRB hosts, e.g., extensive presupernova mass loss and rotation and jets associated with the explosion, we speculate that the recoil of the compact central object, with a velocity of 330 km s^{-1}, may have rendered the jet unstable. In such cases the jet rapidly becomes baryon loaded, if not truncated altogether. Although unlikely to have produced a gamma-ray burst, the jets in Cas A suggest that such outflows may be common features of core-collapse SNe.

Subject headings: gamma rays: bursts — ISM: jets and outflows — supernova remnants — supernovae: individual (Cassiopeia A)

1. INTRODUCTION

The speculation that gamma-ray bursts, or a subset thereof, might be connected with core-collapse supernovae (SNe) was initiated by the coincidence of SN 1998bw with GRB 980425 (Galama et al. 1998) and has been reinforced in recent years by the connections between SN 2001ke and GRB 011121 (Garnavich et al. 2003), SN 2003dh and GRB 030329 (Hjorth et al. 2003), and SN 2003lw and GRB 031203 (Malesani et al. 2004). Spectroscopy of the afterglows of GRB 011211 (Reeves et al. 2002, 2003; Rutledge & Sako 2003; Butler et al. 2005) and of GRB 030227 (Watson et al. 2003) suggest the presence of highly charged ions of Mg, Si, S, Ar, and Ca, but not Fe, Co, or Ni (although Ni may be present in GRB 011211). Claims of the detection of spectral lines in the afterglows of GRB 001025A and GRB 010220 also exist (Watson et al. 2002), although both these gamma-ray bursts lack definitive SN connections. More recently, however, Sako et al. (2005) have questioned the statistical significance of these gamma-ray burst (GRB) afterglow line identifications. It is against the background of these exciting developments that we turn our initial attention in analysis of the 1 Ms *Chandra* observation of the Cassiopeia A supernova remnant to the polar regions, with their striking "jetlike" morphologies. We are motivated to examine in detail the spectra of ejecta knots in the so-called jet regions with a view to determining whether these regions are indeed due to an asymmetric explosion and not just due to cavities in an asymmetric circumstellar medium, and if they are due to jets, whether or not we can infer energetics and other parameters connected with the jet nature.

Ideas that core-collapse supernovae, particularly those occurring after extensive presupernova mass loss as Type Ib/c, might be inherently asymmetrical have also gathered force following SN 1987A (see, e.g., Wang et al. 2002 and references therein). Linear polarizations of optical light of the order of a few percent are typically seen, suggesting nonspherical scattering stellar envelopes, with aspect ratios as large as 2. Mechanisms by which core-collapse supernovae become asymmetrical generally derive from the rotation of the progenitor, which as it collapses may or may not produce strong magnetic field by a magnetorotational instability. A comprehensive review of recent work in this area is given by Wheeler & Akiyama (2005). Such ideas are appealing in the context of Cassiopeia A, since rotating core collapse and the associated magnetic fields (e.g., Proga et al. 2003; Proga 2005; Akiyama et al. 2003) or anisotropic neutrino emission (e.g., Yamasaki & Yamada 2005) are often suggested as a means of producing bipolar outflows or jets. Before proceeding further in this direction, we need to be sure that the morphology we refer to as "jets" really is due to a feature of the explosion and is not arising as a result of cavities in the circumstellar medium at the appropriate locations. Blondin et al. (1996) model the latter situation, and elongated structures of supernova ejecta resembling jets are easily produced. Cas A is inferred to have undergone extensive mass loss from its original $20–25\ M_{\odot}$ progenitor, to have been only $3–4\ M_{\odot}$ upon explosion (Laming & Hwang 2003; Chevalier & Oishi 2003). In addition, the surrounding remnant stellar wind is relatively dense and slow moving. Such conditions do not generally arise with a radiatively driven wind from a $20–25\ M_{\odot}$ progenitor (Woosley et al. 1993), but require the existence of a binary companion to aid the mass loss. In such a case one might expect a departure from spherical symmetry in the wind, from the binary orbital plane to the rotation axis, as is apparent in the case of SN 1987A (Sonneborn et al. 1998).

In this paper we use spectra from the newly acquired deep *Chandra* observation to investigate the properties of the polar regions. We describe the data and methods of analysis in § 2. In § 3 we demonstrate that models of the polar regions based on a

[1] E. O. Hulburt Center for Space Research, Naval Research Laboratory, Code 7674L, Washington DC 20375; laming@nrl.navy.mil.
[2] NASA Goddard Space Flight Center, Code 662, Greenbelt MD 20771; and Department of Physics and Astronomy, Johns Hopkins University, 3400 Charles Street, Baltimore, MD 21218; hwang@orfeo.gsfc.nasa.gov.
[3] Institute for Experimental Physics, University of Debrecen, Bem tér 18/a, Debrecen, H-4026, Hungary.
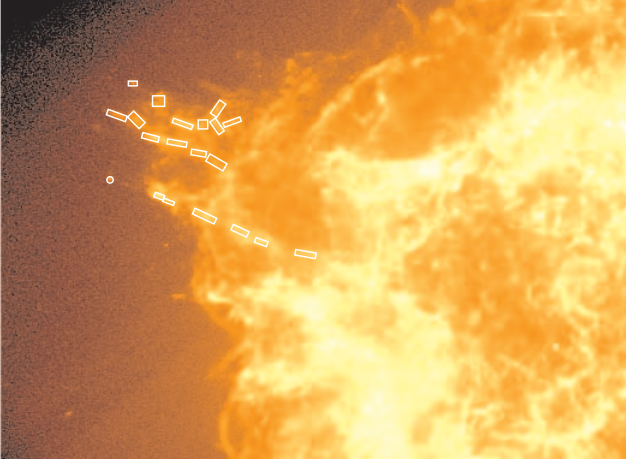
FIG. 1.—Regions of the three filaments (north, middle, and south) of the northeast jet used for spectral analysis.

circumstellar cavity to explain the morphology cannot reproduce the observed spectra and that we really are seeing the evolution into the remnant phase of a bipolar explosion. Section 4 discusses the nature of these jets in more detail, and § 5 concludes.

2. OBSERVATIONS AND DATA ANALYSIS

We use spectra of the polar regions of Cas A from the *Chandra Observatory* Very Large Project (VLP) 1 Ms observation. These data were taken with the backside-illuminated S3 CCD chip of the Advanced CCD Imaging Spectrometer (ACIS) in nine observation segments, mostly over two weeks in 2004, as described in more detail in Hwang et al. (2004). The data were corrected for the time-dependent gain across the S3 chip but could not be corrected for charge transfer inefficiency because the photon events were graded on board the spacecraft prior to data telemetry.

Several regions along the three main filaments of the northeast jet were chosen for spectral analysis, as shown in Figure 1, as well as the composite of the two main filaments of the much fainter counterjet in the southwest (see Hwang et al. 2004). The southernmost filament in the northeast is the straightest and longest of the three and extends farthest into the interior of the remnant. Of particular interest are the very faint knots at the very outer tip of the northeast jet filaments that are newly revealed by the deep *Chandra* observation. Their spectra are shown in Figure 2.

All the spectra were extracted individually for each of the nine observation segments, and corresponding detector response files were generated using CIAO, version 3.0.2.[4] The individual spectra were then added together to produce the final spectrum for a particular region, while the individual response files were weighted according to the relative exposure time of each observation segment before being added to produce the final response files. The time-dependent accumulation of soft X-ray-absorbing contaminant on the ACIS detector was modeled during spectral fitting with the ACISABS model component. The detector gain was adjusted to optimize the fits, compensating in part for
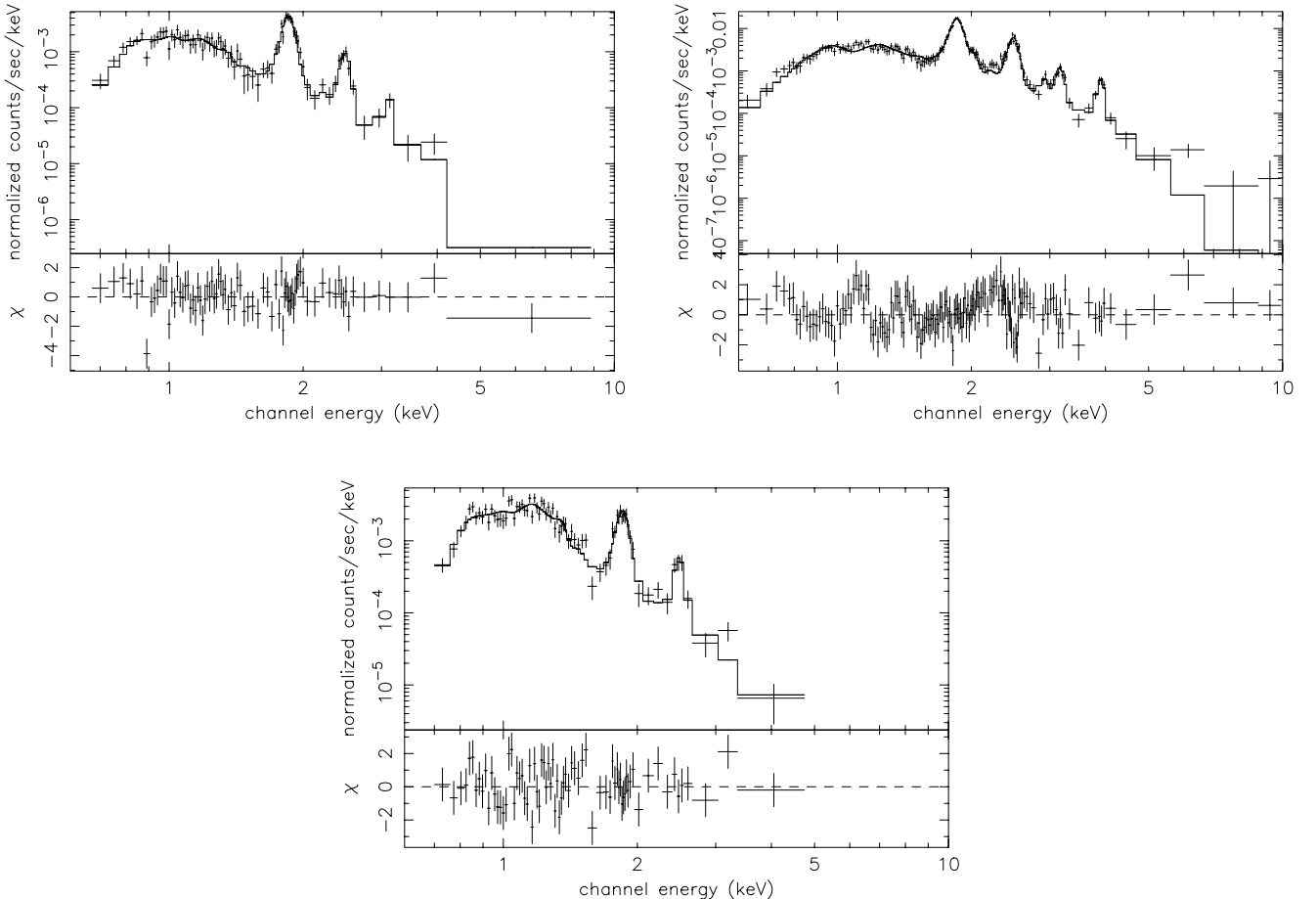
[4] See http://cxc.harvard.edu/ciao.

FIG. 2.—Spectra of the outermost jet knots (north at top left, middle at top right, and south at bottom).

TABLE 1
NEI Models for Jet Tip Knots with O Continuum

Region	Counts	Region Size	χ^2/dof	N_H	kT	$n_e t$	Si	Fe
N tip	3134	4.2×2.2	78.5, 1.11	1.2	0.60 (0.55–0.66)	1.6E13 (>1.4E13)	2200 (1170–4000)	640 (250–1600)
M tip	9626	9.5×2.7	187.9, 1.36	1.3	0.73 (0.70–0.75)	9.6E12 (>4.6E12)	2.3 (1.6–2.6)	0.44 (0.26–0.59)
S tip	2895	$r = 1.5$	92.2, 1.40	1.38 (1.30–1.46)	0.60 (0.58–0.62)	9.4E12 (>6.5E12)	3.1 (1.5–672)	4.2 (2.1–673)

uncertainties in the energy scale, due to both detector performance and the intrinsic bulk motion of the gas.

The goal of the spectral analysis is to obtain the electron temperature, ionization age (the integral of electron density over time since shock passage for the reverse shocked ejecta, assuming a constant electron temperature during this time), and element abundances. We follow Laming & Hwang (2003) in fitting the spectra with models for single-temperature plasmas with time-dependent ionization (nonequilibrium ionization or NEI). We also experimented with collisional ionization models, NEI models with multiple components, and NEI models with a range of ionization ages (mimicking plane-parallel shocks). For the knots along the main body of the jet filaments, the spectral fits were generally improved by using a plane-parallel shock (pshock) model compared to a single NEI component. Two-component NEI models were also an improvement, but generally did not perform better than the pshock models. It is noteworthy that the knots at the very tip of each jet filament have spectra that are well described with a single component (although this is at least partly because these spectra contain fewer counts). The ionization ages fitted for the jet tip spectra are very high, and they may also be successfully fitted with collisional ionization equilibrium models (see Table 1). All the jet region spectra show strong emission lines of Si and S. Those with sufficient counts also show Ar and Ca, as well as Fe K emission. Except for the rather extended knot at the tip of the middle northeast filament, the jet tip spectra are effectively cut off at around 5 keV.

There are various possibilities as to which elements contribute to the continuum. Following Laming & Hwang (2003), we generally model the continuum as coming from either ionized O or Si, with an O continuum consistently giving a better fit (those results are given in Tables 1 and 2). On the basis of χ^2 alone, however, it is not possible to confidently distinguish between the various continuum models. The assumption of which light elements provide the continuum does not strongly affect the quality of the spectral fits but does affect inferences concerning the electron densities and masses in the knot. H continuum models, for example, require higher densities and masses than those with O continuum.

Given the complexity of the spectral models required for most of the jet knots, it is helpful to examine properties of the line emission to assess qualitative trends in the data. In particular, we are interested in possible trends that might be present with location along the jet in the line ratios or line equivalent widths. We therefore fitted the spectra with line blends of individual elements and a bremsstrahlung continuum, as summarized in Table 3. We illustrate in Figure 3 the two strongest trends that we found. The first panel shows the Fe K equivalent width (EW) plotted against the projected distance of the jet region from the point source near the center of the remnant. With the exception of the knots at the very tip of the jet (where the temperatures are significantly lower than elsewhere along the jet, limiting both the emissivity of and sensitivity to Fe K), the Fe K line strength is seen to either stay

roughly level or increase with distance outward along the jet filament. The northern filament in particular appears to show the strongest tendency for an outward increase in Fe K line strength. Although the line strength of Fe K is affected by a number of factors, this trend appears to be echoed in the fitted Fe abundances as well. The second panel of the figure shows the correlation between Ca He α EW and Fe K EW. The Ca He α blends in the jet knots are unusually prominent compared to other regions of the remnant (Hwang et al. 2000) and are seen to roughly follow the Fe K line strength along the jet filaments.

In the jet models discussed below, a significant fraction of reverse shocked jet plasma has now cooled by radiation and adiabatic expansion to temperatures such that it would no longer emit X-rays. The extrapolation of the observed equivalent width trends to larger distances outward along the jet is consistent with such models. If the element composition of the currently unseen jet tip material were dominated by Fe, as would be consistent with its origin deep inside the progenitor, then the radiative cooling time of such plasma would be even shorter than for the O-dominated composition assumed so far, allowing it to cool very quickly.

3. CIRCUMSTELLAR CAVITIES OR EJECTA JETS?

3.1. Circumstellar Cavities

The bipolar morphology exhibited in Cas A has two plausible origins. Both a symmetric explosion into an asymmetric circumstellar medium and an asymmetric explosion into a symmetric medium could produce jetlike structures. The first possibility has been considered by Blondin et al. (1996). In core-collapse supernovae, asymmetries in the circumstellar density may arise from non–spherically symmetric presupernova mass loss, as has been established in the case of SN 1987A. The high degree of mass loss in Cas A inferred from the dynamics (Laming & Hwang 2003) and the likelihood that such winds were driven by the interaction of the progenitor with a binary companion lend support to this idea.

We simulate the evolution of the ionization balance for a knot with a composition resembling that in the middle jet tip knot discussed above, i.e., an O : Si : Fe of 0.82 : 0.13 : 0.05 by mass. The departure from spherical symmetry means that forward shocked circumstellar plasma at the head of the jet moves nonradially (i.e., tangentially) away from the apex, with the consequence that the contact discontinuity at the apex is now much closer to the forward shock. Hence, the forward shock in the polar region should be close to the outermost X-ray-emitting ejecta, at about 3.8 pc, giving an aspect ratio of 3.8/2.5 = 1.5, taking the equatorial forward shock radius as 2.5 pc. Such an aspect ratio agrees best with a density contrast of a factor of 8 between equatorial and polar regions (see Figs. 3 and 4 in Blondin et al. 1996). Accordingly, we take our equatorial core-envelope model from Laming & Hwang (2003), with an outer envelope power-law density profile with an exponent of 9 and a uniform-density inner

TABLE 2
pshock Spectral Fits for Jet Knots with O Continuum

Region	Gain Factor	χ^2/dof	$N_{\rm H}$	kT	$n_e t$	Si	Fe
			North Filament, pshock				
jet3.............	1.001	254.4, 1.30	1.57 (1.51–1.64)	2.32 (2.09–2.56)	2.1E11 (1.8–2.6E11)	1.2 (0.96–1.5)	0.68 (0.56–0.90)
j4	0.999	338.4, 1.54	1.29 (1.28–1.32)	2.00 (1.89–2.13)	2.4E11 (2.2–2.7E11)	1.1 (1.0–1.2)	0.58 (0.52–0.67)
j5b	0.997	224.3, 1.32	1.18 (1.13–1.21)	1.26 (1.15–1.48)	5.6E11 (3.4–9.0E11)	0.56 (0.48–0.61)	0.23 (0.19–0.26)
j5e.............	0.999	194.8, 1.11	1.20 (1.14–1.21)	1.74 (1.59–1.94)	2.5E11 (2.1–2.9E11)	0.96 (0.84–1.0)	0.52 (0.40–0.55)
j5c.............	0.999	428.2, 2.25	1.18	1.40	2.4E11	1.1	0.50
j5a.............	0.999	347.7, 1.61	1.17 (1.14–1.20)	2.79 (2.51–2.96)	2.1E11 (1.9–2.5E11)	0.68 (0.58–0.72)	0.28 (0.24–0.30)
			North Filament, NEI				
jet3.............	1.001	350.6, 1.79	1.65 (1.59–1.70)	2.15 (1.93–2.35)	1.1E11 (9.4E10–1.2E11)	2.1 (1.2–18)	1.0 (0.75–38)
j4	1.000	670.8, 3.05	1.25	1.85	1.1E11	1.1	0.51
j5b	0.997	273.2, 1.61	0.86 (0.77–0.96)	1.07 (1.03–1.15)	5.1E11 (3.5–6.4E11)	0.45 (0.38–0.49)	0.91 (0.07–0.12)
j5e.............	0.999	275.9, 1.57	0.81 (0.75–0.85)	1.15 (1.13–1.21)	3.8E11 2.7–4.5E11)	0.54 (0.46–0.58)	0.13 (0.10–0.14)
j5c.............	1.001	693.4, 3.65	1.03	1.24	1.2E11	0.73	0.24
j5a.............	1.003	589.0, 2.73	1.04	3.55	6.0E10	0.49	0.18
			Middle Filament, pshock				
j8	0.998	240.0, 1.26	1.49 (1.45–1.54)	1.96 (1.91–2.17)	1.5E11 (1.4–1.6E11)	1.5 (1.3–1.9)	0.58 (0.50–0.70)
j10	0.999	285.7, 1.43	1.28 (1.26–1.30)	1.62 (1.53–1.79)	1.8E11 (1.6–2.3E11)	1.8 (1.5–1.9)	0.69 (0.52–0.71)
j11.............	0.998	254.8, 1.32	1.22 (1.16–1.26)	1.83 (1.68–2.03)	2.7E11 (2.3–3.4E11)	1.5 (1.2–1.8)	0.50 (0.41–0.61)
j11a............	1.000	270.3, 1.26	1.26 (1.21–1.28)	1.86 (1.76–1.98)	2.5E11 (2.2–3.1E11)	0.73 (0.66–0.76)	0.26 (0.20–0.28)
			Middle Filament, NEI				
j8	0.998	315.3, 1.66	1.33 (1.28–1.39)	1.85 (1.58–2.00)	7.8E10 (7.0E10–1.0E11)	1.1 (0.90–1.2)	0.33 (0.22–0.36)
j10	0.998	421.4, 2.11	1.20	0.99	4.2E11	2.0	0.57
j11.............	0.998	348.4, 1.81	0.86 (0.80–0.92)	1.20 (1.16–1.26)	3.9E11 (3.2–4.6E11)	0.89 (0.78–1.0)	0.15 (0.13–0.20)
j11.............	0.999	375.3, 1.75	0.79 (0.78–0.81)	1.26 (1.24–1.37)	3.4E11 (3.2–3.9E11)	0.51 (0.49–0.52)	0.066 (0.057–0.074)
			South Filament, pshock				
j13a...........	1.006	358.4, 1.66	1.39 (1.35–1.43)	2.12 (2.05–2.30)	1.5E11 (1.3–1.6E11)	1.7 (1.6–1.9)	0.26 (0.23–0.31)
j13b	1.009	229.6, 1.26	1.50 (1.47–1.55)	1.96 (1.79–2.13)	1.0E11 (9.2E10–1.1E11)	1.2 (1.1–1.3)	0.24 (0.20–0.26)
j18	1.008	493.6, 1.61	1.47 (1.46–1.49)	1.95 (1.85–1.98)	1.8E11 (1.7–1.9E11)	0.28 (0.27–0.29)	0.11 (0.10–10.)
j19	1.008	518.9, 1.87	1.37 (1.35–1.39)	2.32 (2.22–2.42)	1.8E11 (1.7–1.9E11)	0.50 (0.47–0.52)	0.19 (0.17–0.20)
j20	1.008	450.8, 1.91	1.21 (1.19–1.25)	2.27 (2.11–2.40)	2.1E11 (1.9–2.4E11)	0.74 (0.68–0.78)	0.18 (0.15–0.20)
j21	1.008	421.9, 1.60	1.20 (1.17–1.22)	1.68 (1.61–1.76)	4.3E11 (3.9–4.9E11)	0.59 (0.57–0.63)	0.15 (0.13–0.16)

TABLE 2—*Continued*

Region	Gain Factor	χ^2/dof	N_H	kT	$n_e t$	Si	Fe
South Filament, NEI							
j13a............	1.005	469.5, 2.16	1.21	2.08	7.3E10	1.1	0.15
j13b	1.004	308.3, 1.69	1.36	1.85	5.8E10	0.88	0.14
			(1.31–1.40)	(1.73–2.04)	(5.3–6.7E10)	(0.79–0.92)	(0.11–0.15)
j18	1.007	731.9, 2.39	1.27	2.02	7.3E10	0.23	0.075
j19	1.008	807.6, 2.92	1.20	2.64	6.6E10	0.39	0.13
j20	1.008	771.9, 3.27	1.02	2.87	6.6E10	0.56	0.10
j21	1.008	567.7, 2.16	0.72	1.58	2.0E11	0.37	0.037
Counterjet, pshock							
cjet............	1.000	315.7, 1.36	2.06	1.26	4.1E11	1.22	1.2
			(2.04–2.11)	(1.24–1.29)	(3.8–4.5E11)	(1.17–1.43)	(0.97–1.43)
Counterjet, NEI							
cjet............	1.000	427.6, 1.57	1.95	1.08	2.9E11	0.79	0.63
			(1.93–2.03)	(1.05–1.09)	(2.6–3.9E11)	(0.74–1.04)	(0.56–1.00)

core, and reduce the circumstellar density by a factor of 8 in our initial study. By following the evolution of the ionization balance and electron and ion temperatures in the ejecta following reverse shock passage, we compute, and plot in Figure 4, the locus of electron temperature against ionization age for this model, as well as for models with outer envelope power-law exponents of $n = 7$ and 11. The upper branch of each curve corresponds to the phase when the reverse shock is propagating through the constant-density inner ejecta core. The lower branch corresponds to reverse shock propagation through the outer power-law envelope, and the maximum ionization age is found at the uppermost point in each curve at the core-envelope boundary. For

$n = 9$, this is found to be 4.3×10^{11} cm^{-3} s (log $n_e t = 11.6$), with a temperature of 6.5×10^6 K (log $T_e = 6.8$). The other models either give higher ionization age and lower temperature, or the reverse. Comparison with the fit results from § 2, plotted as boxes corresponding to the uncertainties in temperature and ionization age for each knot, shows that no cavity model gives a sufficient density of plasma at a high enough temperature to match the observations. Simply put, the ejecta expand sufficiently rapidly into the cavity that the density is too low either for appreciable electron-ion equilibration to raise the electron temperature or to ionize the plasma to the observed values. The only way to make such a model work would be to include some

TABLE 3
LINE STRENGTHS IN JET KNOTS

| Region	Counts	Region Size	Fe K Centroid	Fe K EW	Ca He α EW	Si He/Ly Ratio	kT
North Filament							
jet3...............	19953	5.7 × 4.9	6.632	4.5 (3.6–5.3)	0.99 (0.83–1.2)	2.7 (2.0–3.5)	0.74,3.4
j4	38989	9.6 × 2.1	6.635	3.7 (3.1–4.3)	0.76 (0.71–0.83)	3.3 (3.1–3.6)	[0.17], 2.4
j5e...............	19120	4.4 × 4.2	6.690	2.4 (1.3–3.3)	1.0 (0.81–1.3)	4.2 (3.2–4.8)	0.45, 3.7
j5a...............	19279	7.5 × 3.5	6.643	2.6 (2.1–3.2)	0.88 (0.68–0.82)	2.2 (1.9–2.4)	1.0, 11
j5c...............	32972	7.2 × 3.2	6.722	2.5 (2.4–2.6)	0.53 (0.45–0.62)	5.7 (4.9–6.7)	0.41, 2.1
j5b	27203	8.4 × 2.1	[6.661, 0.05]	0.9 (0.07–1.7)	0.19 (0.13–0.30)	3.9 (3.0–4.7)	0.58, 1.8
Middle Filament							
j8	23291	7.6 × 4.0	6.592	2.8 (2.0–3.6)	1.2 (1.1–1.4)	6.3 (5.5–7.3)	0.46, 3.7
j10	37045	9.1 × 2.4	6.601	2.3 (1.5–3.1)	1.0 (0.91–1.2)	6.0 (5.6–6.7)	0.55,2.6
j11................	25017	7.0 × 2.6	6.666	2.0 (1.4–2.7)	1.1 (0.93–1.2)	3.5 (3.0–4.0)	0.53, 3.7
j11a..............	29189	9.2 × 3.8	6.626	2.1 (1.6–2.7)	0.64 (0.55–0.72)	3.3 (3.0–3.8)	0.61, 2.9
South Filament							
j13a.............	39392	4.6 × 2.2	6.605	1.7 (1.1–2.1)	0.76 (0.68–0.83)	4.2 (4.1–4.5)	1.8, 80
j13b	20171	5.3 × 1.6	[6.610, 0.1]	1.3 (0.3–1.7)	0.43 (0.36–0.51)	6.6 (6.0–7.7)	
j18	74142	11.2 × 2.9	6.645	0.58 (0.44–0.73)	0.10 (0.08–0.12)	4.0 (3.8–4.3)	1.7, [150]
j19	62144	8.0 × 2.8	6.686	1.2 (1.0–1.4)	0.17 (0.15–0.20)	3.1 (3.0–3.3)	1.7, [150]
j20	44787	6.0 × 2.3	6.676	1.7 (1.3–2.1)	0.22 (0.18–0.28)	2.8 (2.7–3.0)	1.6, [100]
j21	60072	9.7 × 2.6	6.648	1.3 (0.95–1.5)	0.11 (0.09–0.14)	2.7 (2.5–2.8)	1.6, [150]
Counterjet							
cjet..............	60518		6.597	4.0 (3.0–5.1)	0.37 (0.30–0.45)	4.4 (3.4–5.3)	0.39, 1.86
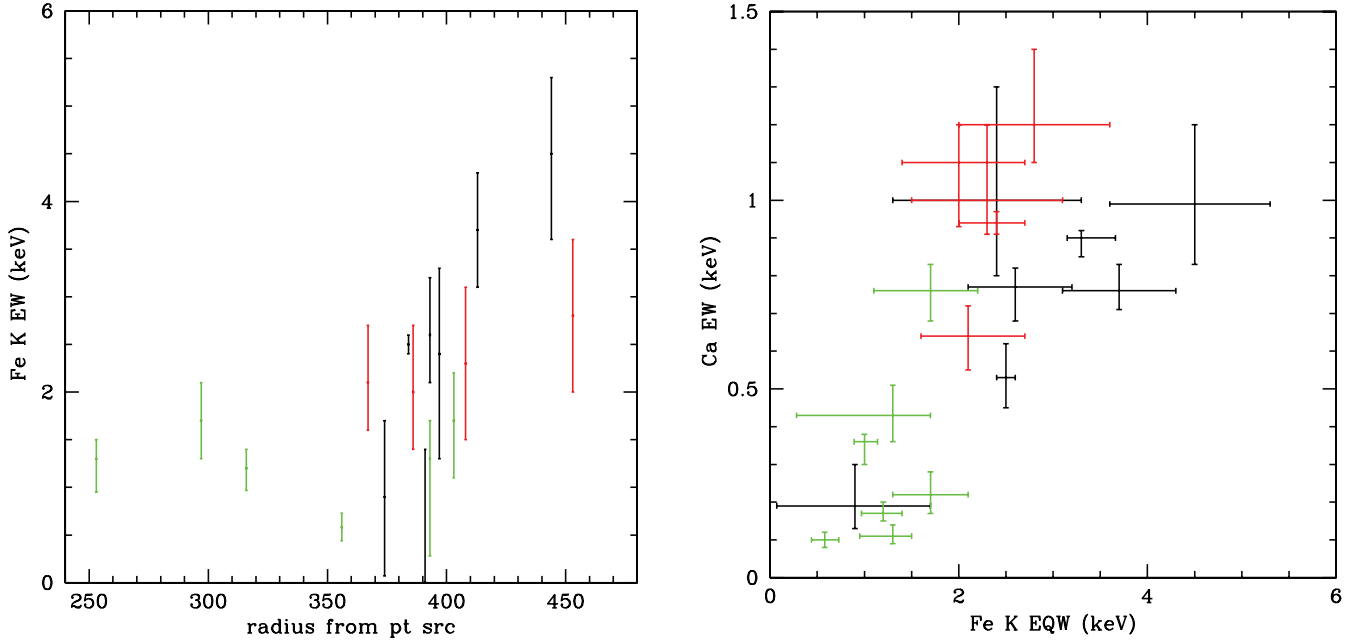
Fig. 3.—Fe K equivalent width plotted for knots in the north (*black*), middle (*red*), and south (*green*) jet filaments as a function of the distance of the center of the extraction region relative to the position of the Cas A point source near the center of the remnant. The correlation of Ca EW compared to Fe EW is shown in the panel to the right.

collisionless electron heating at the reverse shock (currently neglected; see Laming & Hwang 2003 and references therein for fuller discussion of this point), which with reference to Figure 4 could provide the extra factor of 3 or so in electron temperature required to match the observations of knots in the jet "stem," but those at the jet tip would still be discrepant.

3.2. Jets

We model jets based on the simulation of Khokhlov et al. (1999). These authors studied the explosion of the inner 4.1 $M_\odot$
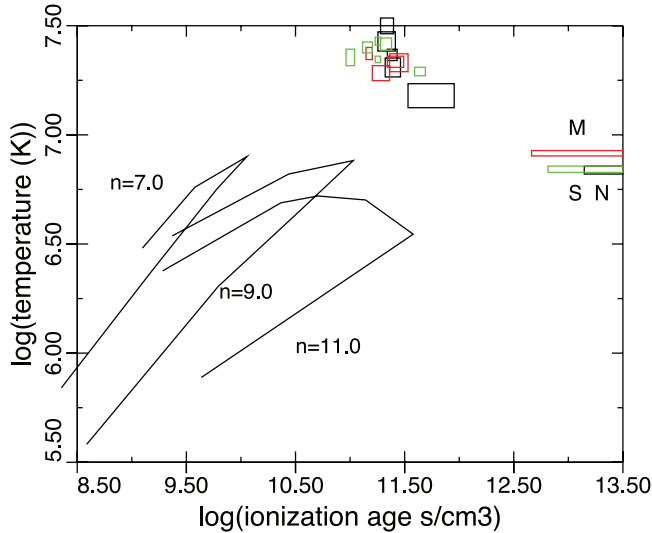

Fig. 4.—Loci on the electron temperature–ionization age plane of fitted knots in the northeast jet, color coded such that knots from the middle filament are red, knots from the south filament are green, and those from the north filament are black. Also plotted are curves derived from models or circumstellar cavities for ejecta profiles corresponding to a uniform-density core and a power-law outer envelope, $\rho \propto r^{-n}$, with $n = 7$, 9, and 11. The discrepancy between observations and models suggests that circumstellar medium cavity models cannot be responsible for the jet morphology.

of a 15 $M_\odot$ progenitor (assuming substantial presupernova mass loss), induced by baryonic jets emanating from the central regions of the star, where the composition is dominated by Fe and Si. The inner 1.6 $M_\odot$ is assumed to fall back onto a proto–neutron star, and the remaining 2.5 $M_\odot$ of ejecta should give a reasonable match to the parameters of Cas A. Initially, each jet comprises about 0.05 $M_\odot$ of material, and together they have 9×10^{50} ergs of kinetic energy. The jet power is constant for the first 0.5 s and is ramped down to zero after another 1.5 s. The equivalent isotropic mass and energy in the jet when they are launched would be 2 $M_\odot$ and 2×10^{52} ergs, respectively, increasing to 8 $M_\odot$ and 8×10^{52} ergs upon jet breakout. From the radius of the jet at launch compared to its final radius upon emergence through the stellar surface, we infer a jet density profile $\rho_j \propto 1/r$, which also matches the figures presented by Khokhlov et al. (1999). We use an adaptation of the BLASPHEMER code (Laming & Grun 2002; Laming & Hwang 2003) that implements the solutions for ejecta profiles $\rho \propto r^{-n}$ with $n < 3$ given by Truelove & McKee (1999) and is summarized here in Appendix A. A jet unconfined by the surrounding ejecta would obey $\rho_j \propto 1/r^2$.

In Figure 5 we plot the locus of electron temperature and ionization age for jet models assuming 2.3×10^{52} ergs equivalent isotropic energy and 1.815 $M_\odot$ ejecta mass. The ejecta mass is taken from that determined in the polar region exterior to the jet by Laming & Hwang (2003). The energy is modified slightly from the value used by Khokhlov et al. (1999) to give better agreement with the observed morphology. Specifically, we want the faint X-ray knots observed at the very tip of the jet to end up at a radius of approximately 3.8 pc from the explosion center. The models differ in that abundance sets of O : Si : Fe are taken from the fits to the three jet tip knots, color coded as black for the north tip, 0.004 : 0.628 : 0.368; red for the middle tip, 0.82 : 0.13 : 0.05; and green for the south tip, 0.55 : 0.12 : 0.33. In addition, we have also computed a model appropriate for the north tip, where half the plasma is assumed to be H. This is given by the black dotted line. As can be seen, the jet models give a reasonable match to both the collisional ionization equilibrium knots at the jet tip, as well as the NEI knots further
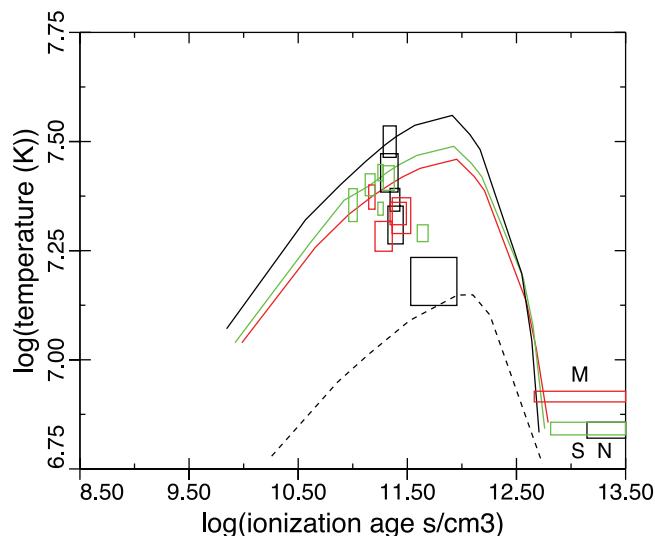
Fig. 5.—Same fitted jet knots as in Fig. 4, compared with jet models specified to match the fitted abundances in the knots at the jet tips, as solid lines with the same color coding. Small differences in the onset of thermal instability are visible, due to the different abundance sets. The black dashed line shows the result of assuming half the plasma in the N filament to be H dominated. This reduces the electron temperature by over a factor of 2, but the onset of thermal instability is less sudden. Jet models appear to match the data points much better.

down the jet stem, in terms of ionization age and electron temperature. Some of the jet stem knots fall at lower temperatures than modeled assuming O to be the most abundant element, but which could be understood if the jet knot plasma comprises a substantial fraction of H. Of course, the abundances in the jet stem knots are probably not the same as those in the three tip knots, although here they have been modeled as such. The variation between the three curves for north, middle, and south jet filaments should give some idea as to the variation to be expected as abundances vary within reasonable limits.

As well as comparing electron temperatures and ionization ages coming from our models with those from fits, we have also investigated the ionization balance predicted by the models for Fe and Si in the jet tip knots. Figure 6 shows the model Fe and Si charge state distributions for ejecta that went through the reverse shock at various times between 1.3 and 1.6 yr after explosion, compared with the charge state distribution of a plasma in collisional ionization equilibrium at 8.6×10^6 K (*thin solid line*), meant to match the conditions in the jet tip knot of the middle filament. For both Fe and Si, the model charge states corresponding to an electron temperature of 8.6×10^6 K are a poor match to the observed charge states, with too many ions in high charge states, e.g., Fe^{+24} and Si^{+13}. This is because the recombination from these ions is a slow process. Much better correspondence between observation and the models is found for ejecta that have been allowed to cool down to temperatures $(5-6) \times 10^6$ K, i.e., lower than actually observed. We speculate that although we have tried to model and fit the knot spectra as though they are single plasmas, shocked instantaneously by the reverse shock, some inhomogeneity may still exist. Small variations in elemental composition or density are likely to reveal themselves during the onset of thermal instability, when the temperature is decreasing very quickly with time, making the heavy element line emitting regions cooler than the surroundings, which mainly emit continuum. At 1–2 yr after explosion, the reverse shock speed in our models is 4000–5000 km s^{-1}, which means it would take 10^8 s or 3 yr to traverse a knot of $1''$ extent.
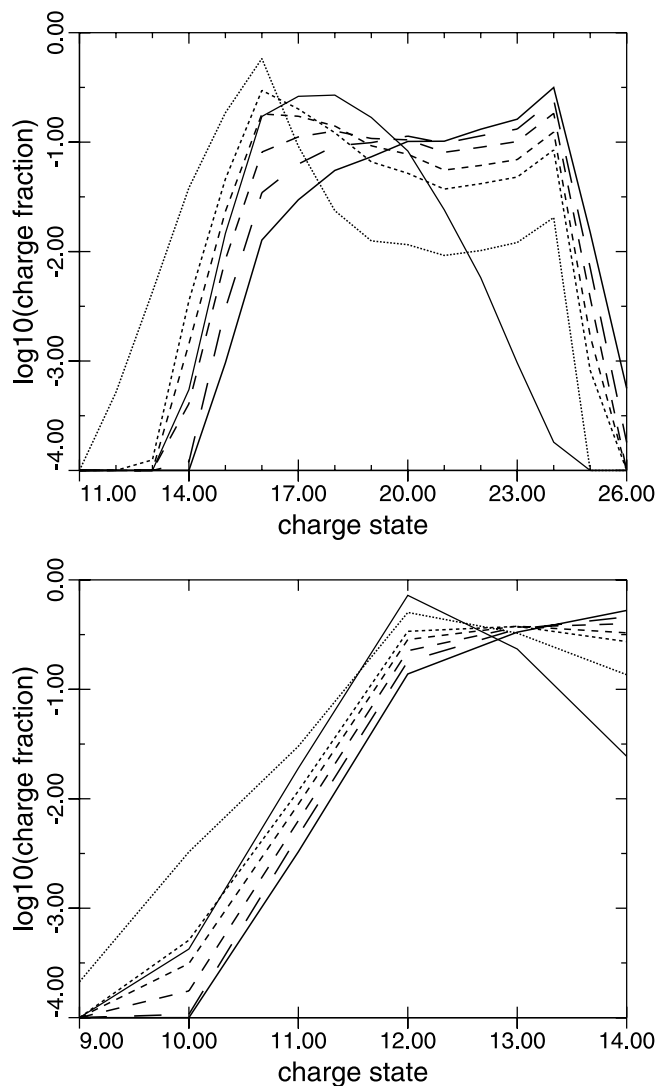

Fig. 6.—Charge state distributions of Fe (*top*) and Si (*bottom*) corresponding to ejecta encountering the reverse shock at different times following explosion. The thick solid line indicates Fe (or Si) going through the reverse shock 1.6 yr after explosion, which gives the best agreement with the fitted electron temperature. The dashed curves with successively finer dashes are for ejecta undergoing reverse shock passage 1.45, 1.4, 1.35, 1.315, and 1.3 yr after explosion, with electron temperatures of 7.84×10^6, 7.04×10^6, 6.17×10^6, 5.51×10^6, and 5.22×10^6 K, respectively. Although these ejecta cool to lower temperatures than indicated by the fits, the charge state distributions are in better agreement with the observations. The thin solid lines indicate the collisional ionization equilibrium charge state distributions for a temperature of 8.6×10^6 K, and are indicative of the actual ionization balance detected in the jet knots.

It is therefore also likely that our assumption that the whole knot is shocked instantaneously breaks down, in that the reverse shock speed evolves as it traverses the knot, making a single ionization age less realistic.

A related problem is that knots in the main body of the jet are better fit by plane-parallel shock models that integrate over a range of ionization ages, rather than by single ionization age models. These knots with smaller ionization ages are shocked later (i.e., around 5–10 yr after explosion) than those at the jet tip, at a time when the reverse shock in our models is evolving much less rapidly with time. These knots are also observed at smaller radii relative to those in the jet tip than our models would predict and have similar problems with the ratios of He-like to H-like Si, in that the models predict much more H-like Si than actually observed. This is quite different from Si in knots of

similar temperature and ionization age studied in Laming & Hwang (2003). The difference lies in the fact that for the jet models considered here, the electron temperature was previously much higher than it is at present, and the plasma is recombining. The NEI models that assume a constant temperature are probably not good approximations. This is quite different from the knots in more equatorial regions in Laming & Hwang (2003), where the postshock knot electron temperature is roughly constant, making the NEI models excellent approximations. We suspect that these knots may have initially undergone an oblique interaction with the reverse shock, leading to a lower peak electron temperatures, and have undergone further interactions with shocks reflected from the blast wave as it encounters clumps (i.e., quasi-stationary flocculi) in the circumstellar medium, which would further decelerate and heat them. Such a scenario does indeed seem to be the case for SN 1987A (Zhekov et al. 2005), in that a variety of shock conditions are required to fit the *Chandra* LETG (Low Energy Transmission Grating) spectra, and indeed should be expected as the blast wave begins to encounter the inner ring of circumstellar material, producing a succession of shocks reflected back into the following ejecta.

3.3. *Related Issues*

Our conclusion that we are indeed seeing an asymmetric explosion into a symmetric medium is based solely on the spectroscopy of knots in the polar regions. Laming & Hwang (2003), using similar techniques for ejecta knots observed elsewhere in the remnant, concluded that the explosion energy per unit solid angle was higher in regions close to the jet than in more equatorial directions. A completely independent conclusion of similar anisotropy in the explosion comes from a survey of the outlying optical knots by Fesen (2001). These optical knots are generally taken to be essentially undecelerated by their interaction with the circumstellar plasma, and hence any velocity variation exhibited by these knots must have an origin in the explosion itself, so that our conclusion is in line with those of other researchers.

However, considerable uncertainty surrounds the mechanism(s) of formation of the various kinds of optical knots, so here we briefly offer some speculations as to how these features fit in with the hydrodynamic models for Cas A studied in Laming & Hwang (2003). Knots rich in nitrogen are observed around the remnant (but not apparently in the northeast jet region) expanding with a velocity of about 10,000 km s^{-1}. Due to their composition, they must originate in the outer layers of ejecta. We suggest that these knots are the end result of a Rayleigh-Taylor (R-T) instability at the contact discontinuity. In simulations, R-T fingers of ejecta typically do not penetrate through the forward shock, but Jun et al. (1996) show that in the presence of a clumpy external medium, this is not the case. The R-T fingers can gain extra kinetic energy from the vortices generated by the shock-cloud interactions. In this case we would expect the velocity with which the resulting clumps of nitrogen-rich material expand to be similar to the ejecta expansion velocity at the core-envelope boundary, which in the models of Laming & Hwang (2003) is indeed around 10,000 km s^{-1}. Knots rich in oxygen and its burning products (they also show prominent S II emission) are found in various regions of the remnant, especially in the northeast jet. Many authors have surmised that these arise as a result of the "Fe bubble" effect, whereby Ni-Co-Fe bubbles inflated by the energy deposition due to the radioactive decay of Ni to Co and ultimately to Fe compress the surrounding plasma. This argument would suggest that Fe should be present, or should have been present in the jet regions in order to produce the fast-

moving knots observed there today. We return to the subject of Fe in the jets below.

Finally, the location and velocity of the reverse shock in the northwest and southwest regions of the remnant have been inferred from optical observations with *HST* (*Hubble Space Telescope*) WFPC2 (Wide Field Planetary Camera 2) images taken in 2000 and 2002 (Morse et al. 2004). The reverse shock radius of ~1.8 pc and velocity with respect to the freely expanding ejecta of ~2000 km s^{-1} correspond reasonably well with the $n = 9$ model from Laming & Hwang (2003), which predicts a reverse shock radius of 1.7 pc and velocity of 1500 km s^{-1}. The ejecta free expansion velocity in this model is 4800 km s^{-1}, to be compared with 5000 km s^{-1} in Morse et al. (2004). Adjusting the model of Laming & Hwang (2003) to better match, say, the faster reverse shock velocity (e.g., by decreasing the ejecta envelope power-law index to $n = 7$) would make the discrepancy between the measured and modeled reverse shock radii worse, and vice versa. We would expect the models to slightly underestimate the reverse shock velocity at 340 yr, since Laming & Hwang (2003) make the approximation of holding the reverse shock velocity constant during its propagation through the uniform-density ejecta core, whereas in fact we would expect it to slowly accelerate. Consequently, the reverse shock velocities computed at earlier times in the remnant evolution for a given model should be more accurate than those for the current epoch. In any case, the reverse shock is observed to be fragmented and irregular in morphology due to local density inhomogeneities and may even be dynamically unstable, so we consider the agreement between our model and the *HST* observations to be satisfactory.

4. DISCUSSION

4.1. *Jet, Mass, Energy, and Opening Angle*

We first discuss in more detail the nature of the Truelove & McKee (1999) $n = 1$ models employed to simulate the jet emission. The equivalent isotropic energy of 2.3×10^{52} ergs is chosen to place ejecta cooling through temperatures of 0.7 keV at a distance of about 3.8 pc from the explosion center. These models predict a blast wave radius at the jet tip of 5.66 pc and a velocity of 7850 km s^{-1}. For reasons to be discussed below, these are probably overestimates, but we do not actually detect the location of the blast wave anywhere in the jet region. This radius, however, is not too far off from the radius of the outermost optical knot in the jet of 4.8 pc (Fesen 2001). The gas that we see today at a 0.7 keV temperature encountered the reverse shock between 1 and 2 yr after explosion and has a mass coordinate of about 0.5. This means that nearly half the ejecta went through the reverse shock during these first 1–2 yr and has by now cooled to temperatures below those where it would be visible in X-rays to *Chandra*. Consequently, in the jet there should be a lot of cold plasma at the jet head, cooled by both radiative losses and adiabatic expansion.

To our knowledge, there are no published simulations of jet explosions carried through to the supernova remnant phase of the evolution. However, we can get some idea of the hydrodynamics involved in the interaction of a jet with an ambient medium from recent laboratory work (Blue et al. 2005; Foster et al. 2005; Lebedev et al. 2005). Here we can clearly see a jet stem, such as we plausibly observe in X-rays in Cas A, and a denser "mushroom cap" jet tip, which in Cas A has presumably cooled to too low a temperature to be visible in X-rays. From Figure 5 it appears that the knots at the jet tip are on the verge of becoming radiatively unstable. Radiatively cooled ejecta at the
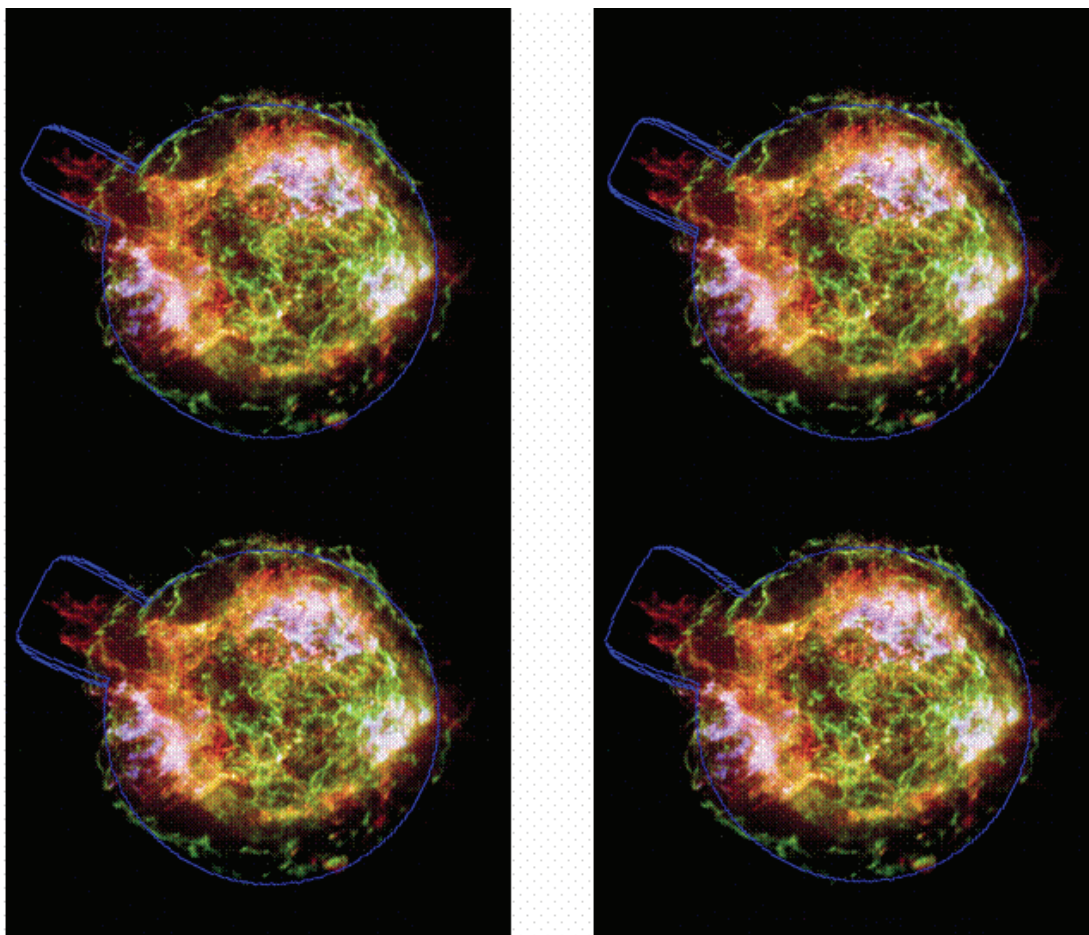
Fig. 7.—Illustrative plots of the blast wave profile in the northeast jet region for jet models with a uniform energy core and a power-law outer region, $E \propto \theta^{-n}$, with $n = 2, 3,$ and 8 (based on Lazzati & Begelman 2005; Zhang et al. 2004; Graziani et al. 2005, respectively), for uniform energy core opening angles of $5°$ (*top left*), $7°$ (*top right*), $9°$ (*bottom left*), and $11°$ (*bottom right*).

jet tip will reduce the pressure driving the forward shock, so that the forward shock radius and velocity might be expected to be smaller than in the adiabatic models of Truelove & McKee (1999).

As mentioned above, we do not detect the blast wave in the northeast jet region. Elsewhere in the remnant it is easily identifiable as a rim of continuum emission, presumably synchrotron emission from cosmic-ray electrons. The width of this rim is identified as being due to the radiative loss time of the cosmic-ray electrons as they are advected away from the shock (Vink & Laming 2003), with the result that the magnetic field must be of the order of 0.1 mG, presumably amplified from a very low value in the presupernova stellar wind by a cosmic-ray precursor, as suggested by Bell & Lucek (2001) and Lucek & Bell (2000). Why is such emission absent from the jet region? One possibility is that the shock here is oblique; the inflowing and outgoing plasma do not flow along the shock normal, and diffusive shock acceleration is known to be less efficient in such cases (e.g., Drury 1983), leading to lower cosmic-ray energies and weaker magnetic field amplification by the cosmic-ray precursor. It is also possible that the blast wave at the jet tip is actually outside the *Chandra* field of view.

Our simulations of the knot spectra above give the equivalent isotropic energy in the jet as 2.3×10^{52} ergs, with the assumption that the jet equivalent isotropic mass is 1.815 $M_\odot$, as determined from knots at the jet base by Laming & Hwang (2003). We are,

however, unable to independently constrain the jet mass in the same way, since as mentioned above, we do not detect the blast wave driven by the jet. The plot of electron temperature against ionization age is essentially independent of the jet mass and energy, so long as these are constrained to place plasma cooling through a temperature of about 700 eV at a radial distance from the explosion center of about 3.8 pc. A higher jet mass (as in, e.g., Khokhlov et al. 1999) would of course require a higher jet energy, but we consider this an unlikely possibility. We have made estimates of the plasma density and mass in the knots at the jet tip from the spectral fits, which generally come out *lower* than our model values. While there is considerable uncertainty in these estimates, they suggest that if anything the jet has a density similar to or less than that of the surrounding stellar envelope and is not overdense, as in the case modeled by Khokhlov et al. (1999).

Given an equivalent isotropic energy in the jet of 2.3×10^{52} ergs, the evaluation of the total jet energy requires some knowledge of the opening angle. In Figure 7 we overlay blast wave profiles including the northeast jet estimated from a "pseudo-Kompaneets" approximation outlined in Appendix B. We assume that sufficient cold ejecta, either shocked or unshocked, exists in the jet region so that the remnant retains some "memory" of the initial energy distribution. We take the jet energy profile to be constant within the jet opening angle and to fall off as $E \propto \theta^{-n}$ outside this region. We consider values of n of

2, 3, and 8, coming from values favored by Lazzati & Begelman (2005), Zhang et al. (2004), and Graziani et al. (2005), respectively. The panels show the cases of jet opening angles of $5°$ (*top left*), $7°$ (*top right*), $9°$ (*bottom left*), and $11°$ (*bottom right*), and in each case the $n = 8$ model is the narrowest and $n = 2$ the widest. The total jet energy evaluates to about 10^{50} ergs, taking an opening angle of $7°$. This is nearly an order of magnitude lower than the "standard" gamma-ray burst radiated energy found by Frail et al. (2001), probably much lower than the kinetic energy of relativistic ejecta in such events, and argues against Cas A actually having produced a gamma-ray burst during its explosion. This energy, with the likely jet underdensity compared to the surrounding stellar envelope, also suggests that the jets are unlikely to have induced the explosion, being significantly less energetic than those in the simulation of Khokhlov et al. (1999). More likely they are the by-product of an explosion proceeding by different means.

Our estimation of blast wave profiles around the jet region assumed that at all times in the evolution of Cas A there has been sufficient cold ejecta at the jet head to retain some "memory" of the initial explosive energy distribution with angle. In § 2 we described how the equivalent width of the Fe K feature is seen to increase with radial distance, especially in the northern filament, a trend that if extrapolated would suggest that the jet tip regions are dominated in composition by Fe. This would shorten the radiative cooling time for shocked ejecta over that calculated assuming O-dominated composition and support our assumptions here. Hwang & Laming (2003) estimate that only a few percent of the total mass of Fe that Cas A is expected to have ejected is currently visible as X-ray-emitting ejecta, and so a significant portion of the unseen jet material could also be composed of Fe. A number of authors (Wang et al. 2002; Nagataki et al. 1998, 2003) have also suggested that bipolar jets should be locations where α-rich freezeout occurs with correspondingly large abundances of ^{44}Ti. In the X-ray-emitting portion of the northeast jet, we see rather little Fe, and certainly no knots that may be considered as pure Fe as found by Hwang & Laming (2003). We have searched for inner shell line emission from ^{44}Sc and ^{44}Ca (the decay products of ^{44}Ti, formed mainly by K shell electron capture) in the region at the head of the jet, where we expect the X-ray dark ejecta to be, without success. Our (3σ) upper limit is about 4 photons, less than 0.1% of the ^{44}Sc inner shell line emission expected to be observed in the whole remnant, based on the gamma-ray line observations of nuclear de-excitation in ^{44}Sc (Vink et al. 2001; Vink & Laming 2003) and ^{44}Ca (Iyudin et al. 1994; Schönfelder et al. 2000).[5] We should caution that the regions we investigated are right at the edge of the *Chandra* ACIS field of view and that regions that underwent α-rich freezeout may even be farther out.

4.2. *Could Cas A Have Produced a GRB?*

As mentioned above, although Cas A was produced in an explosion that accelerated jets of material, the effects of which persist to this day, the energetics of these features make it unlikely that Cas A actually produced a gamma-ray burst. In this section we discuss how other features of the Cas A supernova remnant (SNR) might reinforce this conclusion.

The Cas A explosion energy, in the range $(2-4) \times 10^{51}$ ergs, places it clearly as a supernova and not a hypernova, although

an observer placed on the jet axis (equivalent isotropic energy of 2.3×10^{52} ergs) might have perceived it as such from line broadening (Mazzali et al. 2002; Ramirez-Ruiz & Madau 2004). Wang (1999) identified possible hypernova remnants in M101, supporting the suggestion (Paczynski 1998; MacFayden & Woosley 1999) that such a class of highly energetic explosions exists. Furthermore, Atoyan et al. (2006) identify a source detected only in TeV gamma rays by HESS (High Energy Stereoscopic System) as the remnant of a gamma-ray burst, based on theoretical arguments. As Ramirez-Ruiz & Madau (2004) discuss, the absence of a Compton-scattered jet component (i.e., scattering photons from a misaligned jet into an observer's line of sight) in otherwise normal Type Ibc SNe would suggest that those hosting GRBs are not normal Type Ibc SNe, supporting the conjecture that Type Ibc SNe hosting gamma-ray bursts constitute a separate class of more energetic SNe, known as hypernovae. However, more recently Soderberg et al. (2006) presented evidence that the optical properties of Type Ibc SNe associated with GRBs are not significantly different from "normal" Type Ibc events and that GRB-associated SNe can only be reliably identified from their radio signatures. Nagataki et al. (2006) show that ^{56}Ni production in a GRB jet would be insufficient to power a hypernova and that if these explosions exist as a separate class, ^{56}Ni must be produced elsewhere in the ejecta, further loosening any association between hypernovae and jets.

Podsiadlowski et al. (2004) and van Putten (2004) estimate the branching ratio from Type Ibc supernovae to gamma-ray bursts to be in the range 10^{-3} to 10^{-2}. Podsiadlowski et al. (2004) suggest that special evolutionary circumstances are required to lead to an explosion of the hypernova type and the accompanying gamma-ray burst, presumably involving a specific type of binary interaction to give the required rotation rate and mass loss. Van Putten (2004) identifies the small branching ratio with the probability of the central compact object remaining at the explosion center and accreting material to become a high-mass black hole. This argument would suggest that Cas A, which produced what is presumably a neutron star recoiling with a velocity in the plane of the sky of 330 km s^{-1} (Thorstensen et al. 2001), could not have produced a gamma-ray burst. Aside from these statistical arguments, the recoiling neutron star should naturally be expected to destabilize the jets, causing rapid baryon loading and quenching any nascent gamma-ray burst.

We have verified that the explosion center determined from the positions and velocities of the X-ray knots cataloged by Delaney et al. (2004) is consistent with that determined from optical observations by Thorstensen et al. (2001), although the uncertainties in the X-ray position are considerably larger than those in the optical work. In this case the central compact object recoil is at about $75°$ to the jet axis. According to Wang et al. (2006), the recoil component perpendicular to the jet axis requires either a relatively slow rotation rate upon explosion, rather unlikely in our view, since such a case appears unlikely to generate jets, or the presence of a binary companion. A binary companion is also favored to produce the required degree of presupernova mass loss (Young et al. 2006), and so this is the scenario we prefer.

Additional circumstantial evidence against Cas A hosting a gamma-ray burst lies in the apparent absence of stellar wind circumstellar media in most gamma-ray burst afterglows modeled to date (Chevalier & Li 2000; Panaitescu & Kumar 2002), with Piro et al. (2005) identifying one of the few (GRB 011121) consistent with a stellar wind density profile. Of course, Cas A shows clear evidence of expanding into a remnant stellar wind, consistent with only a minority of gamma-ray bursts. The Cas A

---

[5] A detected gamma-ray flux of $(2-3) \times 10^{-5}$ photons cm^{-2} s^{-1} gives 20–30 photons cm^{-2} in 10^6 s, which combined with the ACIS HMRA (High Resolution Mirror Assembly) effective area gives total detected photons in the range $5 \times 10^3 - 10^4$ in the remnant as a whole.

explosion also seems to have been extraordinarily dim, possibly due to being shrouded in a dense stellar wind at the time of explosion, although Young et al. (2006) comment that the dust component of the wind, if the Cas A progenitor evolved as a Wolf-Rayet star, is unlikely to have significantly changed the interstellar extinction from values found today.

Mazzali et al. (2005) report the observation of the Type Ic supernova SN 2003jd, which appears to be an intermediate case between normal Type Ic SNe and gamma-ray burst host SNe. No gamma-ray burst is noted, but the supernova is clearly asymmetrical, exhibiting double-peaked [O I] lines. These are interpreted as coming from equatorial regions of the progenitors, while emission from the polar regions is dominated by jets. More recently, Folatelli et al. (2006) and Tominaga et al. (2005) report similar conclusions for SN 2005bf, another energetic Type Ib/c supernova. We suggest that the explosion of Cas A may have been a similar event. It is clearly asymmetrical, with a little more mass in equatorial than in polar regions (taking the estimates of Table 5 in Laming & Hwang 2003 at face value), presumably the result of polar jets forcing the overlying stellar envelope to lower latitudes. However, the degree of asymmetry produced appears to be at the low end of that predicted by models, and the jets themselves are clearly less energetic than in either the simulations of Khokhlov et al. (1999) or observations of gamma-ray bursts (Frail et al. 2001).

5. CONCLUSIONS

We have studied the northeast polar region of the Cas A SNR in considerable detail. In contrast, the counterjet region appears to be expanding into a more complex circumstellar medium, possibly a cloud of higher density, which limits the conclusions we may draw. Fits to knots in the counterjet are completely consistent with those in the northeast jet stem. However, the high ionization age knots at the tip of the northeast jet, which turn out to be of crucial importance for the analysis in this paper, have no counterparts in the counterjet. It is also worth commenting that the three jet tip knots studied in detail here are simply not visible on images from the earlier 50 ks *Chandra* observations of Cas A. The deep 1 Ms VLP observation was absolutely necessary to see these at all. Analyses of the knots reveal that the "jetlike" morphology really is due to an explosive jet and is not arising as a result of interaction with a cavity or lower density region in the circumstellar medium. While Cas A exhibits many of the properties suggested for gamma-ray burst hosts, extensive presupernova mass loss and jets presumably requiring nonnegligible rotation of the progenitor, the jet itself is inferred to be significantly less energetic than generally accepted for gamma-ray bursts and so is unlikely to have actually been a gamma-ray burst itself. Any pair or Poynting flux dominated jet is likely to have become

baryon loaded if the jet was destabilized by the recoil of the neutron star, giving rise to the ejecta-dominated structure that we see today. Furthermore, the jet is also significantly less energetic than in the jet-induced explosion model of Khokhlov et al. (1999), suggesting that the supernova giving rise to the Cas A remnant was not a jet-induced explosion. This is supported by Laming & Hwang (2003), who find evidence of asymmetry in the explosion at the low end of or below the range generally modeled or invoked to explain polarization observations of Type Ibc or Type II supernovae. Consequently, we believe we are seeing jets produced as a by-product of an explosion that proceeded by other means, e.g., a more usual neutrino-generated event, and that evidence of convective overturn in the ejecta should be interpreted in terms of these types of models (e.g., Kifonidis et al. 2000, 2003) rather than the rotating jet-powered models (e.g., Akiyama et al. 2003).

This work only scratches the surface of the analysis to be done and the physics to be extracted from the Cas A VLP data set. In subsequent papers we intend to analyze in detail the ejecta knots, with particular emphasis on the Fe-rich regions. Using methods developed in Laming & Hwang (2003) and Hwang & Laming (2003), together with observed knot velocities, both from proper motions in the plane of the sky and from Doppler shifts, we plan to reconstruct a three dimensional distribution of ejecta knots. With this in hand, we then envisage studying various explosion models to gain insight into the mechanisms and instabilities involved by comparison with our catalog of knots.

Note added in manuscript.—Our attention has been drawn recently to the coincidence of GRB 060218 and SN 2006aj. SN 2006aj is estimated to have ejected 2 $M_\odot$, with energy 2 × 10^{51} ergs (Mazzali et al. 2006), very similar to our previous inferences for the explosion that caused Cas A. The accompanying GRB 060218 is very low energy (10^{49}–10^{50} ergs equivalent isotropic energy; Campana et al. 2006), signifcantly lower than the jet energy inferred for Cas A. We stress that our conclusions in the present paper are drawn with respect to "classical" long GRBs, with typical energies $\sim 10^{51}$ ergs, and not with respect to a putative class of low-energy GRBs seen predominantly in the local universe, of which GRB 980425 and GRB 031203 are also examples (Cobb et al. 2006).

APPENDIX A

JET MODELS IN BLASPHEMER

In Laming & Hwang (2003) and Hwang & Laming (2003) we used core-envelope solutions given by Truelove & McKee (1999) for trajectories of the forward and reverse shocks, where the ejecta density distribution is taken to be represented by a uniform-density core with an outer power-law envelope $\rho \propto r^{-n}$, where $n > 5$. Here we outline our implementation of the Truelove & McKee (1999) solutions for power-law ejecta density distributions $\rho \propto r^{-n}$ with $n < 3$, which have no constant-density core, expanding into a circumstellar medium with $\rho \propto r^{-s}$. For reasons given in the main text, we expect these to be better representations of the jet regions, taking $s = 2$ as in Laming & Hwang (2003). We use the same system of units as in Laming & Hwang (2003).[6] Other parameters are the

---

[6] The numerical factors in eqs. (A1) and (A2) in Laming & Hwang (2003) for the $s = 0$ ambient medium are in error; they should be 473.6 and 3.43 instead of 423 and 3.07, respectively.

lead factor $l_{ED} = 1.1 + 0.4/(4 - s)$, the ratio of forward to reverse postshock pressures $\phi_{ED} = 0.343(1 - s/3)^{0.43}$, and the expansion velocity of the outermost ejecta $v_{ej} = 2[(5 - n)/(3 - n)]^{1/2}$.

The blast wave trajectory for $n < 3$ ejecta during the ejecta-dominated phase is given by

$$t = \frac{R_b}{v_{ej}l_{ED}} \left[1 - \left(\frac{3 - n}{3 - s} \right) \sqrt{\frac{\phi_{ED}}{l_{ED}f_n}} R_b^{(3-s)/2} \right]^{-2/(3-n)}. \tag{A1}$$

We define a transition time to Sedov-Taylor behavior as follows. The blast wave radius at the transition is estimated from $v_b = R_b/t = 2\sqrt{\xi}R_b^{(s-3)/2}/(5 - s)$, with $t = R_b/v_{ej}l_{ED}$ yielding $R_{conn} = [v_{ej}l_{ED}(5 - s)/2\sqrt{\xi}]^{2/(s-3)}$. The transition time is then calculated from equation (A1) with R_{conn}, where $\xi = [(5 - s)(10 - 3s)/8\pi]^{1/2}$. For $t < t_{conn}$, R_b is calculated from equation (A1), $R_r = R_b/l_{ED}$,

$$v_b = \frac{R_b}{t} \left\{ \frac{1 + [(n - 3)/(3 - s)]\sqrt{\phi_{ED}/(l_{ED}f_n)}R_b^{(3-s)/2}}{1 + [(n - s)/(3 - s)]\sqrt{\phi_{ED}/(l_{ED}f_n)}R_b^{(3-s)/2}} \right\}, \tag{A2}$$

and $v_r = R_r/t - v_b/l_{ED}$. For $t > t_{conn}$,

$$R_b = \left[R_{conn}^{(5-s)/2} + \sqrt{\frac{(5 - s)(10 - 3s)}{8\pi}}(t - t_{conn}) \right]^{2/(5-s)},$$

$$v_b = \left[\frac{1}{v_b(t_{conn})} + \frac{5 - s}{2(R_b - R_{conn})^{(s-3)/2}} \sqrt{\frac{8\pi}{(5 - s)(10 - 3s)}} \right]^{-1},$$

$$R_r = \left[\frac{R_{conn}}{l_{ED}t_{conn}} - v_r \ln\left(\frac{t}{t_{conn}} \right) \right] t,$$

$$v_r = \frac{R_{conn}}{l_{ED}t_{conn}} - \frac{v_b(t_{conn})}{l_{ED}}, \tag{A3}$$

where the reverse shock velocity is held constant, similar to the core propagation phase in Laming & Hwang (2003). In this approximation, if $R_r/t < 0.75v_r$, then the reverse shocked ejecta flows backward toward the remnant center. In this case we set the expansion velocity of reverse shocked ejecta equal to zero, and hence

$$R_r = 0.75v_r t = \left[\frac{R_{conn}}{l_{ED}t_{conn}} - v_r \ln\left(\frac{t}{t_{conn}} \right) \right] t, \tag{A4}$$

giving $t = t_{conn} \exp(r_{conn}/l_{ED}t_{conn} - 0.75)$, and so

$$R_r = 0.75v_r t_{conn} \exp\left(\frac{R_{conn}}{l_{ED}t_{conn}v_r} - 0.75 \right), \tag{A5}$$

and then $v_r = 0.75R_r/t$. While a little ad hoc, this gives good agreement with the $s = 0$ models given in Truelove & McKee (1999). We emphasize that the jet ejecta in which we are most interested undergo reverse shock passage with $t < t_{conn}$, and so the reverse shock velocity is given accurately by equation (A1) and those in the text immediately following. The later behavior of v_b and R_b is only necessary for the adiabatic expansion of these shocked knots.

The remaining parameter required is the separation between the forward shock and the contact discontinuity. In a jet, this can be significantly smaller than the value obtained in a spherically symmetric explosion, because plasma entering the forward shock in the jet region is shocked obliquely, and its postshock flow is no longer radial. We set this distance equal to zero in our simulations, so that the contact discontinuity is at the forward shock.

We have also updated the atomic data for dielectronic recombination of K-shell and L-shell ions. Recombination from H- to He-like and from He- to Li-like ions is taken from Dasgupta & Whitney (2004). The successive isoelectronic sequences of Li-, Be-, B-, C-, N-, O-, and F-like ions are taken from Colgan et al. (2004; see also Colgan et al. 2005), Colgan et al. (2003), Altun et al. (2004; see also Altun et al. 2005), Zatsarinny et al. (2004a), Mitnik & Badnell (2004), Zatsarinny et al. (2003; see also Zatsarinny et al. 2005), and Gu (2003), respectively. In addition, dielectronic recombination from Ne- to Na-like and from Na- to Mg-like ions is taken from Zatsarinny et al. (2004b) and Gu (2004).

APPENDIX B

THE KOMPANEETS APPROXIMATION

We give a treatment of the Kompaneets approximation for Cas A, following Bisnovatyi-Kogan & Silich (1995), in the case of a uniform explosion into a nonuniform circumstellar density distribution. We then comment on the modifications necessary to treat asymmetric explosions into symmetric circumstellar media. The fundamental assumption leading to the Kompaneets approximation

is that for an explosion into asymmetric media, the pressure behind the blast wave is constant with position on the shock surface. Defining the shock surface by $f(r, \theta, t) = 0$ in conditions of azimuthal symmetry, we have

$$\frac{df}{dt} = \frac{\partial f}{\partial t} + \frac{\partial f}{\partial r}\frac{\partial r}{\partial t} + \frac{\partial f}{\partial \theta}\frac{\partial \theta}{\partial t} = \frac{\partial f}{\partial t} + \nabla f \cdot \boldsymbol{v} = 0. \tag{B1}$$

Writing $|\nabla f| = [(\partial f/\partial r)^2 + (\partial f/r\partial\theta)^2]^{1/2}$ and $|\boldsymbol{v}| = [(\gamma + 1)P_{\rm sh}/2\rho]^{1/2} = [(\partial r/\partial t)^2 + (r\partial\theta/\partial t)^2]^{1/2}$, we get

$$\left(\frac{\partial r}{\partial t}\right)^2 = \frac{(\gamma + 1)P_{\rm sh}}{2\rho}\left[1 + \left(\frac{1}{r}\frac{\partial r}{\partial\theta}\right)^2\right]. \tag{B2}$$

We assume a density profile $\rho = \rho_0 \exp(\theta/W)(r_0/r)^s$, where ρ_0 and r_0 are the values of ρ and r at some fiducial point, taken here to be the head of the jet, and set $y = t[(\gamma + 1)P_{\rm sh}/2\rho_0]^{1/2}$, so that

$$\frac{r_0^s}{r^s}\left(\frac{\partial r}{\partial y}\right)^2 = \left[1 + \left(\frac{\partial \ln r}{\partial\theta}\right)^2\right]\exp\left(-\frac{\theta}{W}\right). \tag{B3}$$

At this point we remark that a postshock pressure variation of $P = P_0 \exp(-\theta/W)$ and a uniform ambient density would be mathematically identical. However, such a pressure variation needs to be sustained somehow, since otherwise with a high postshock sound speed the pressure behind the blast wave should equilibrate. We have already seen that in the jet region, shocked circumstellar plasma encounters the blast wave obliquely and once shocked, flows nonradially away from the jet tip. Consequently, one might expect the dynamics of the forward shock in the jet region to remain ejecta dominated well past the time that the forward shock elsewhere in the remnant has evolved to the Sedov-Taylor phase. The cooling time of shocked ejecta at the jet tip is also sufficiently short to render the sound speed at the jet tip slow and hence impede the pressure equilibration among the shocked ejecta. Therefore, we assume that the expanding jet "remembers" the anisotropy of explosion energy well into the remnant phase and calculate blast wave profiles from the corresponding modification of the Kompaneets approximation.

We define $\xi = (r_0/r)^{s/2}\partial r/\partial y = \partial r_0/\partial y$, evaluated at $\theta = 0$ but also assumed to be independent of θ below, rearrange, and integrate to find

$$\ln r = \pm \int \sqrt{\xi^2 \exp(\theta/W) - 1}\, d\theta + \ln \int \xi\, dy, \tag{B4}$$

and hence

$$\frac{\partial \ln r}{\partial\xi} = \pm \int \frac{\xi \exp(\theta/W)}{\sqrt{\xi^2 \exp(\theta/W) - 1}}\, d\theta + \frac{\partial}{\partial\xi}\ln \int \xi\, dy = \pm \frac{2W}{\xi}\left[\sqrt{\xi^2 \exp\left(\frac{\theta}{W}\right) - 1} - \sqrt{\xi^2 - 1}\right] + \frac{\partial}{\partial\xi}\ln \int \xi\, dy. \tag{B5}$$

Setting $\xi = \cosh x$ and $\int \xi\, dy = r_0$, we can integrate to find

$$\frac{1}{2W}\ln\left(\frac{r}{r_0}\right) = -\sqrt{\xi^2 \exp\left(\frac{\theta}{W}\right) - 1} + \arctan\left[\sqrt{\xi^2 \exp\left(\frac{\theta}{W}\right) - 1}\right] + \sqrt{\xi^2 - 1} - \arctan\left(\sqrt{\xi^2 - 1}\right), \tag{B6}$$

where the negative sign has been taken. If the normal to the shock front makes an angle α to the radial direction, then $\partial \ln r/\partial\theta = \tan \alpha$ and $\tan^2\alpha = \xi^2 \exp(\theta/W) - 1$.

Lazzati & Begelman (2005) give a preferred angular dependence of $dE/d\Omega \propto \theta^{-2}$ outside of a central region of constant energy. This is derived from considerations of the gamma-ray burst jet-cocoon structure at jet breakout from the stellar envelope and also reproduces the so-called Frail correlation. In this case our Kompaneets approximation becomes

$$\frac{r_0^s}{r^s}\left(\frac{\partial r}{\partial y}\right)^2 = \left[1 + \left(\frac{\partial \ln r}{\partial\theta}\right)^2\right]\frac{W^2}{\theta^2}. \tag{B7}$$

Following the steps above, we derive

$$\ln\left(\frac{r}{r_0}\right) = \pm \frac{\xi}{W}\left[\frac{\theta}{2}\sqrt{\theta^2 - \frac{W^2}{\xi^2}} - \frac{W^2}{2\xi^2}\ln\left|\theta + \sqrt{\theta^2 - \frac{W^2}{\xi^2}}\right|\right]_{\theta=W}^{\theta=\theta}$$

$$= \pm \frac{\xi}{W}\left[\frac{\theta}{2}\sqrt{\theta^2 - \frac{W^2}{\xi^2}} - \frac{W^2}{2\xi^2}\ln\left|\theta + \sqrt{\theta^2 - \frac{W^2}{\xi^2}}\right| - \frac{W^2}{2}\sqrt{1 - \frac{1}{\xi^2}} + \frac{W^2}{2\xi^2}\ln\left|W + W\sqrt{1 - \frac{1}{\xi^2}}\right|\right]. \tag{B8}$$

Simplified expressions in the limit $1/\xi^2 \to 0$ or $\xi \sim 1$ and $\theta \gg W$ are $r = r_0 \exp(-\xi\theta^2/2W)$ and $r = r_0(2\theta/W)^{W/2} \exp(-\theta^2/2W)$, respectively. Zhang et al. (2004) prefer $n = 3$, and Graziani et al. (2005) prefer $n = 8$. These cases require numerical integration of the corresponding version of equation (B7).

REFERENCES

Akiyama, S., Wheeler, J. C., Meier, D. L., & Lichtenstadt, I. 2003, ApJ, 584, 954
Altun, Z., Yumak, A., Badnell, N. R., Colgan, J., & Pindzola, M. S. 2004, A&A, 420, 775
———. 2005, A&A, 433, 395
Atoyan, A., Buckley, J., & Krawczynski, H. 2006, ApJ, 642, L153
Bell, A. R., & Lucek, S. G. 2001, MNRAS, 321, 433
Bisnovatyi-Kogan, G. S., & Silich, S. A. 1995, Rev. Mod. Phys., 67, 661
Blondin, J. M., Lundqvist, P., & Chevalier, R. A. 1996, ApJ, 472, 257
Blue, B. E., et al. 2005, Phys. Rev. Lett., 94, 095005
Butler, N., Ricker, G., Vanderspek, R., Ford, P., Crew, G., Lamb, D. Q., & Jernigan, J. G. 2005, ApJ, 627, L9
Campana, S., et al. 2006, Nature, submitted (astro-ph/0603279)
Chevalier, R. A., & Li, Z. 2000, ApJ, 536, 195
Chevalier, R. A., & Oishi, J. 2003, ApJ, 593, L23
Cobb, B. E., Bailyn, C. D., van Dokkum, P. G., & Natarajan, P. 2006, ApJ, submitted (astro-ph/0603832)
Colgan, J., Pindzola, M. S., & Badnell, N. R. 2004, A&A, 417, 1183
———. 2005, A&A, 429, 369
Colgan, J., Pindzola, M. S., Whiteford, A. D., & Badnell, N. R. 2003, A&A, 412, 597
Dasgupta, A., & Whitney, K. G. 2004, Phys. Rev. A, 69, 022702
Delaney, T., Rudnick, L., Fesen, R. A., Jones, T. W., Petre, R., & Morse, J. 2004, ApJ, 613, 343
Drury, L. O'C. 1983, Rep. Prog. Phys., 46, 973
Fesen, R. A. 2001, ApJS, 133, 161
Folatelli, G., et al. 2006, ApJ, 641, 1039
Foster, J. M., et al. 2005, ApJ, 634, L77
Frail, D. A., et al. 2001, ApJ, 562, L55
Galama, T. J., et al. 1998, Nature, 395, 670
Garnavich, P. M., et al. 2003, ApJ, 582, 924
Graziani, C., Lamb, D. Q., & Donaghy, T. Q. 2005, ApJ, submitted (astro-ph/0505623)
Gu, M. F. 2003, ApJ, 590, 1131
———. 2004, ApJS, 153, 389
Hjorth, J., et al. 2003, Nature, 423, 847
Hwang, U., Holt, S. S., & Petre, R. 2000, ApJ, 537, L119
Hwang, U., & Laming, J. M. 2003, ApJ, 597, 362
Hwang, U., et al. 2004, ApJ, 615, L117
Iyudin, A. F., et al. 1994, A&A, 284, L1
Jun, B.-I., Jones, T. W., & Norman, M. L. 1996, ApJ, 468, L59
Khokhlov, A. M., Höflich, P. A., Oran, E. S., Wheeler, J. C., Wang, L., & Chtchelkanova, A. Yu. 1999, ApJ, 524, L107
Kifonidis, K., Plewa, T., Janka, H.-T., & Müller, E. 2000, ApJ, 531, L123
———. 2003, A&A, 408, 621
Laming, J. M., & Grun, J. 2002, Phys. Rev. Lett., 89, 125002
Laming, J. M., & Hwang, U. 2003, ApJ, 597, 347
Lazzati, D., & Begelman, M. C. 2005, ApJ, 629, 903
Lebedev, S. V., et al. 2005, MNRAS, 361, 97
Lucek, S. G., & Bell, A. R. 2000, MNRAS, 314, 65
MacFayden, A. I., & Woosley, S. E. 1999, ApJ, 524, 262
Malesani, D., et al. 2004, ApJ, 609, L5
Mazzali, P. A., Deng, J., Nomoto, K., Pian, E., Tominaga, N., Tanaka, M., & Maeda, K. 2006, Nature, submitted (astro-ph/0603567)
Mazzali, P., et al. 2002, ApJ, 572, L61
———. 2005, Science, 308, 1284

Mitnik, D. M., & Badnell, N. R. 2004, A&A, 425, 1153
Morse, J. A., Fesen, R. A., Chevalier, R. A., Borkowski, K. J., Gerady, C. L., Lawrence, S. S., & van den Bergh, S. 2004, ApJ, 614, 727
Nagataki, S., Hashimoto, M., Sato, K., Yamada, S., & Mochizuki, Y. 1998, ApJ, 492, L45
Nagataki, S., Mizuta, A., & Sato, K. 2006, ApJ, submitted (astro-ph/0601111)
Nagataki, S., Mizuta, A., Yamada, S., Takabe, H., & Sato, K. 2003, ApJ, 596, 401
Paczynski, B. 1998, ApJ, 494, L45
Panaitescu, A., & Kumar, P. 2002, ApJ, 571, 779
Piro, L., et al. 2005, ApJ, 623, 314
Podsiadlowski, Ph., Mazzali, P. A., Nomoto, K., Lazzati, D., & Cappellaro, E. 2004, ApJ, 607, L17
Proga, D. 2005, ApJ, 629, 397
Proga, D., MacFadyen, A. I., Armitage, P. J., & Begelman, M. C. 2003, ApJ, 599, L5
Ramirez-Ruiz, E., & Madau, P. 2004, ApJ, 608, L89
Reeves, J. N., Watson, D., Osbourne, J. P., Pounds, K. A., & O'Brien, P. T. 2003, A&A, 403, 463
Reeves, J. N., et al. 2002, Nature, 416, 512
Rutledge, R. E., & Sako, M. 2003, MNRAS, 339, 600
Sako, M., Harrison, F. A., & Rutledge, R. E. 2005, ApJ, 623, 973
Schönfelder, V., et al. 2000, in AIP Conf. Proc. 510, 5th Compton Symp., ed. M. L. McConnell & J. M. Ryan (Melville: AIP), 54
Soderberg, A. M., et al. 2006, ApJ, 636, 391
Sonneborn, G., et al. 1998, ApJ, 492, L139
Thorstensen, J. R., Fesen, R. A., & van den Bergh, S. 2001, AJ, 122, 297
Tominaga, N., et al. 2005, ApJ, 633, L97
Truelove, J. K., & McKee, C. F. 1999, ApJS, 120, 299
van Putten, M. H. P. M. 2004, ApJ, 611, L81
Vink, J., & Laming, J. M. 2003, ApJ, 584, 758
Vink, J., Laming, J. M., Kaastra, J. S., Bleeker, J. A. M., Bloemen, H., & Oberlack, U. 2001, ApJ, 560, L79
Wang, C., Lai, D., & Han, J. L. 2006, ApJ, 639, 1007
Wang, L., et al. 2002, ApJ, 579, 671
Wang, Q. D. 1999, ApJ, 517, L27
Watson, D., Jeeves, J. N., Osbourne, J. S., O'Brien, P. T., Pounds, K. A., Tedds, J. A., Santos-Lleó, M., & Ehle, M. 2002, A&A, 393, L1
Watson, D., Reeves, J. N., Hjorth, J., Jakobsson, P., & Pedersen, K. 2003, ApJ, 595, L29
Wheeler, J. C., & Akiyama, S. 2005, in Open Issues in Understanding Core Collapse Supernovae, ed. T. Mezzacappa & G. Fuller (Singapore: World Scientific) (astro-ph/0509484)
Woosley, S. E., Langer, N., & Weaver, T. A. 1993, ApJ, 411, 823
Yamasaki, T., & Yamada, S. 2005, ApJ, 623, 1000
Young, P. A., et al. 2006, ApJ, 640, 891
Zatsarinny, O., Gorczyca, T. W., Korista, K. T., Badnell, N. R., & Savin. D. W. 2003, A&A, 412, 587
———. 2004a, A&A, 417, 1173
———. 2004b, A&A, 426, 699
Zatsarinny, O., Gorczyca, T. W., Korista, K., Fu, J., Badnel, N. R., Mitthumsiri, W., & Savin, D. W. 2005, A&A, 438, 743
Zhang, W., Woosley, S. E., & Heger, A. 2004, ApJ, 608, 365
Zhekov, S. A., McCray, R. M., Borkowski, K. J., Burrows, D. N., & Park, S. 2005, ApJ, 628, L127